JOURNAL OF CATALYSIS **175,** 117–128 (1998)
ARTICLE NO. CA981978

# CO Hydrogenation on a Nickel Catalyst

## II. A Mechanistic Study by Transient Kinetics and Infrared Spectroscopy

M. Agnelli, H. M. Swaan, C. Marquez-Alvarez, G. A. Martin, and C. Mirodatos[1]

*Institut de Recherches sur la Catalyse, CNRS, 2 Avenue Albert Einstein, F-69626, Villeurbanne Cédex, France*
E-mail: mirodato@catalyse.univ-lyon1.fr

Received July 24, 1997; revised December 1, 1997; accepted December 1, 1997

**The CO hydrogenation into methane was studied over a Ni/$SiO_2$ catalyst by means of *in situ* transient techniques (DRIFT, SSITKA) in order to have access to a detailed description of the reacting surface and to understand the ageing process related to the kinetic behaviour at steady state. After an initial period of carbon deposition, fast sintering, and particle smoothing via nickel carbonyl transfer, the reacting surface can be described as a monolayer of nickel carbide, largely covered by CO adspecies with an average bonding stoichiometry of CO/2$Ni_s$. The rate of hydrogenation is controlled by the probability for a hydrogen molecule to collide with an active site formed of one to two adjacent Ni atoms free from adsorbed CO. The concentration of active sites is statistically determined by the CO coverage. Carbon atoms belonging to the carbidic layer associated to the active site are hydrogenated by hydrogen activated on the free Ni atoms. The regeneration of the carbidic layer is in turn ensured by CO dissociation after methane desorption. A rate equation is presented with physically meaningful kinetic parameters.** 

*Key Words:* **methanation; nickel on silica; transient kinetic studies; mechanism; ageing process.**

### INTRODUCTION

The investigation of catalytic systems by means of *in situ* methods under operating conditions is of major importance for a complete description of the active site and of the reaction mechanism (1, 2). The diffuse reflectance infrared Fourier-transform (DRIFT) spectroscopy gives access to the direct observation of the surface in the course of the reaction and the steady state isotopic transient kinetics (SSITK) provide a quantitative evaluation of the active sites under steady-state conditions (1–3).

The reaction of CO hydrogenation into methane is a particularly favourable example for applying these techniques since it combines (i) fast steps such as $H_2$ and CO activation, (ii) surface and bulk accumulation of reactive and less or unreactive species (so-called "spectator"), and (iii) slow processes such as metal sintering (4, 5). However, although several aspects of this model reaction are now well understood, still unsolved problems resulting from the complexity of syngas reactions over transition metal catalysts require further investigations, for which the above-mentioned techniques may provide new insights:

(i) The *in situ* activation of catalysts under syngas atmosphere is an important aspect of catalyst ageing which often determines the steady-state catalytic properties. In this respect, a detailed study of the reaction of CO hydrogenation over Ni/$SiO_2$ catalysts was undertaken and the first part of this work was aimed at investigating the morphology changes of Ni particles under the reaction conditions (5). The Ni sintering was shown to involve nickel transfer from particle to particle via nickel carbonyl species and was modelled according to a modified Ostwald-ripening mechanism. The selective development of ⟨111⟩ planes was revealed after several hours under reaction conditions. The formation of a nickel carbide monolayer was observed simultaneously within the first hours on-stream, possibly interfering with the sintering process. This carbide-like phase being likely to participate directly to the catalytic process, more information about the precise chemistry involved during this startup step is necessary for understanding the catalyst performance under steady-state conditions.

(ii) Several mechanisms and kinetics of the methanation reaction over nickel catalysts have been proposed. They are discussed in a recent paper by Alstrup (4) and the author proposes a micro-kinetic model to account for the literature data obtained by Goodman and co-workers on nickel single crystal surfaces (6). A key parameter such as the coverage of active surface carbon, $\theta_C$, is assumed to be constant for the range of temperature considered, and evaluated to be 0.05 monolayer (ML), which corresponds to the lowest coverage reported in (6). However, much larger carbon accumulation values were found under steady-state conditions, leading

[1] Corresponding author.



0021-9517/98 $25.00

to a $\theta_C$ of 0.38 ML from temperature programmed hydrogenation (TPH) experiments in (5), or as large as several monolayers as reported by Biloen *et al.* (7) from transient experiments. Thus, an utmost important question remains to evaluate the exact concentration of "active" carbon, i.e., to understand the precise relationship which could exist between "active" and "inactive" or "less active" species on the working surface. In other words, it has to be determined if the reaction occurs only on a small number of "special sites" created before the steady state is achieved, which would make the reaction structure sensitive, or if the fraction of active surface does not depend on any crystallographic configuration of the active sites, which would make the reaction structure insensitive.

A second basic assumption in (4) was to consider an identical surface site and stoichiometry, referred as "∗", for any adsorbed intermediate species—CO, H, C, $CH_x$, O, OH. This allows the authors to propose a balance equation between free and occupied surface sites such as

$$\theta_* = (1 - \theta_c)/[1 + (K_1 P_{H_2})^{1/2} + K_2 P_{CO}], \qquad [1]$$

$\theta_c$ being the fraction of active sites occupied by active carbon, $K_1$ and $K_2$ being the equilibrium constant of the elementary steps corresponding to $H_2$ and CO adsorption, respectively. Thus, the overall rate equation was assumed to be a function of $\theta_C$ and $\theta_*$ as

$$\text{rate} = \frac{a_1 P_{H_2}^2 \theta_C \theta_*}{1 + a_2 P_{H_2}^{n/2}}, \qquad [2]$$

$a_1$ and $a_2$ being a function of the rate and equilibrium constants of the elementary steps considered in the model (4).

Another way to consider the formation of active intermediates is the "ensemble model" proposed by Dalmon and Martin in (9), which assumes that the reaction takes place on ensembles composed of several adjacent Ni atoms, free from inactive (undissociated) adsorbed CO, and that the rate is proportional to $(1 - \theta_{CO})^W$, where $\theta_{CO}$ is the CO coverage and W is the number of Ni atoms in the ensemble (nuclearity of the site). The W value, however, could not be calculated since $\theta_{CO}$ was not known under reacting conditions (9).

The present part II of this work on CO hydrogenation over $Ni/SiO_2$ catalysts reports data obtained by *in situ* transient techniques at various stages of the catalyst testing. It aims at investigating the changes in surface reactivity induced simultaneously by morphological changes and carbon deposition. The direct evaluation of surface coverages and active site concentration under reaction conditions is expected to provide a quantitative basis to test the validity of the quoted kinetic models.

## EXPERIMENTAL

### *Catalyst*

The $Ni/SiO_2$ catalyst used in the present study is similar to those described in previous papers (5, 9). The precursor (20 wt% Ni) was obtained by contacting silica (Aerosil Degussa, 200 $m^2 g^{-1}$) with a solution of nickel nitrate hexamine. The solid was dried, then crushed to powder, and reduced at 650°C for 15 h at 2°C/min heating rate in flowing hydrogen (5 liters $h^{-1}$). The average Ni particle size was measured by hydrogen chemisorption, magnetic methods, and electron microscopy and was found to be 4.2 nm after reduction with a good agreement between the three techniques (5).

### *CO Hydrogenation*

The methanation reaction (feed $H_2/CO = 2$) was carried out in the 230–350°C temperature range and at atmospheric pressure in a fixed-bed flow reactor. From gas analyses carried out by on-line gas chromatography (TCD and FID) at the reactor outlet, the selectivity in methane was found to be around 90% (the remaining 10% being higher hydrocarbons and traces of oxygenates) and fairly stable with time on-stream. The degree of conversion was maintained low enough (<10%) to ensure that differential and isothermal conditions were achieved without external diffusion limitation; moreover, the silica support being nonporous, any significant internal diffusion could be discarded. Temperature-programmed hydrogenation (TPH) of the carbon deposits was carried out after various times on $CO/2H_2$ stream at 230°C by flushing the catalyst under He flow, decreasing the temperature to 25°C, then heating under hydrogen flow (1.8 liters/h) up to 650°C at 8°C/min. Only methane was detected around 240°C, from which the amount of deposited carbon was calculated (5).

### *Steady-State Isotopic Transient Kinetics (SSITK)*

The isotopic transient experiments under steady-state conditions were carried out by changing rapidly the composition of the feeding mixture from $^{12}CO + 2H_2$ to $^{13}CO + 2H_2$ or from $^{12}CO + 2H_2$ to $^{12}CO + 2D_2$ and vice versa at the inlet of the micro reactor. The abrupt switch was obtained with an automatic four-way valve located just before the reactor. The signal distortion induced by the noncatalytic system (tubes, reactor, etc.) was followed by the transient signal of a helium trace introduced in one of the feeds. The gas composition at the reactor exit was continuously analysed with a VG mass spectrometer. Details on the technique are reported in (3, 10).

### *$H_2/D_2$ Exchange*

The reaction of $H_2/D_2$ exchange was used for characterising the catalyst: (i) after the initial reduction, (ii) after

given times on CO hydrogenation stream, (iii) after catalyst regeneration by TPH. The exchange was performed at −20°C by admitting an equimolar mixture of $H_2$ and $D_2$ (flow rate of 0.48 liters/h) on the catalyst and measuring the rate of HD formation.

### *Diffuse-Reflectance Infrared Fourier-Transform (DRIFT) Spectroscopy*

Twelve to 13 mg of the $Ni/SiO_2$ precursor sieved to 0.2–0.3 mm were loaded in a DRIFT cell provided by Spectratech and adapted to a Nicolet 550 FTIR spectrometer. The solid was reduced *in situ* in standard conditions with flowing hydrogen. After reduction the solid was cooled down to 230°C, the reaction temperature, purged with a helium flow, and the reacting mixture ($CO + 2H_2$) was flowed at atmospheric pressure through the catalytic bed.

DRIFT spectra were continuously taken during the startup and the ageing period, each spectra consisting of 10 scans with a resolution of 4 $cm^{-1}$. The contribution of each carbonyl band was calculated by assuming a gaussian shape and using the Peakfit programme.

In order to characterise the nickel surface at various stages of the catalyst life, CO was also used as a probe and its adsorption was studied by DRIFT spectroscopy. Spectra were taken at room temperature under a helium flow containing 1% CO and at increasing temperatures without CO:

(i) after reduction at 650°C, outgasing in a helium flow at 300°C, and cooling down to room temperature,

(ii) after 4 h of reaction at 230°C and removal of adsorbed hydrogen by flowing helium at the same temperature,

(iii) after catalyst regeneration by *in situ* TPH.

## RESULTS

### *Catalyst Ageing during Methanation Reaction*

Figure 1 summarises the normalized changes in catalytic activity (curve a) and in metallic surface area (curve b) as a function of time on stream, as detailed in part I of the present study (5). It was deduced from the resemblance between the two curves, a and b, that the metallic surface decay largely contributed to the catalyst deactivation observed under methanation conditions. However, another factor had to be considered to account for the remaining difference between the two curves a and b. The amount of carbon deposits (C atoms/surface Ni atom) was measured after the reaction by TPH. These carbon deposits were found to be hydrogenated into methane at the reaction temperature (as a single peak at around 240°C ) and to interact chemically with the nickel, as proved by magnetic measurements (5). No other types of carbon, such as bulk carbide species, graphite veils, filaments, or carbonaceous

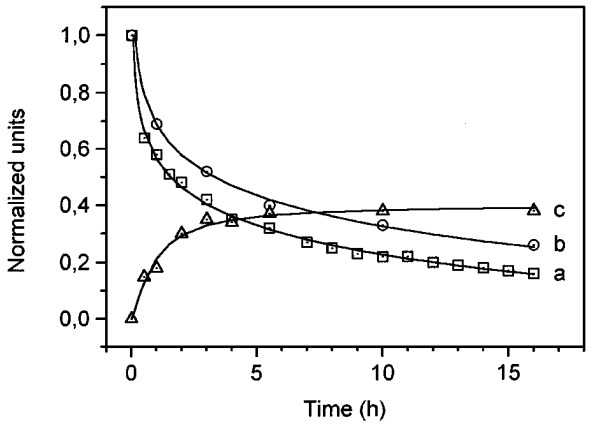


**FIG. 1.** Normalized changes in (a) specific activity, (b) metallic surface, (c) $C/Ni_s$ (deposited carbon atom/surface nickel atom) as a function of time on $CO/2H_2$ stream at 230°C.

species on the silica support, were detected by TPH experiments, which would have been hydrogenated at higher temperature (8). As shown in Fig. 1, curve c, the ratio C/surface nickel atom (accounting for the particle sintering) increased within about 3–4 h on $CO/2H_2$ stream and stabilized at a value of around 0.40 (i.e., 2.5 Ni per C) without any noticeable further evolution. Within the experimental uncertainties and considering the physico-chemical characteristics of that type of carbon (high reactivity towards hydrogen, chemical interaction with metallic nickel), it was proposed that the stabilized $C/Ni_S$ value corresponded to the completion of a monolayer of surface (or subsurface) nickel carbide, $Ni_xC$ ($2 \le x \le 3$). After this initial period, it was considered that the catalyst had reached a pseudo steady-state regime, characterized by a slow and almost constant deactivation.

### *$H_2/D_2$ Exchange at Low Temperature after Reduction, Reaction, and Regeneration*

The specific (per weight unit) and intrinsic (per metallic surface unit) rates of $H_2/D_2$ exchange performed at −20°C at different stages of the catalyst life are reported in Table 1.

**TABLE 1**

**Specific and Intrinsic Rates of $H_2/D_2$ Exchange Carried Out at −20°C on the Fresh, Used, and Regenerated $Ni/SiO_2$ Catalyst**

| Time on CO hydrogenation (h) | Rate of exchange | |
|---|---|---|
| | Specific ($\mu$mol/g s) | Intrinsic ($\mu$mol/$m^2_{Ni}$ s) |
| 0 | 827 | 38 |
| 0.5 | 457 | nd |
| 4 | 11 | 1 |
| After TPH regeneration | 659 | 42 |

*Note.* nd = not determined.

**TABLE 2**

**Comparison between Rates of CO Hydrogenation ($r_H$) and Deuteration ($r_D$) as a Function of Temperature**

| Temperature (°C) | $X_{CH_4}$ (%) | $X_{CD_4}$ (%) | KIE $r_H/r_D$ |
|---|---|---|---|
| 230 | 0.65 | 1.1 | 0.63 |
| 250 | 1.56 | 2.5 | 0.63 |
| 270 | 1.8 | 3.0 | 0.64 |
| 300 | 5.0 | 7.5 | 0.66 |
| 600 | 36.8 | 48.0 | 0.79 |

As can be seen, the rate of exchange decreased after CO hydrogenation by a factor of 2 after 30 min and by almost two orders of magnitude after 4 h on $CO/2H_2$ stream. The intrinsic activity was totally restored after TPH treatment under hydrogen. The apparent activation energies for the $H_2/D_2$ exchange were found to be close to 3–4 kcal/mol for all samples, except for the 4 h aged one for which $E_a$ increased to 9 kcal/mol.

In addition, the rates of CO hydrogenation were compared by substituting $H_2$ by $D_2$, in order to evaluate kinetic isotopic effects (KIE) (Table 2).

As shown in Table 2, the CO deuteration was found to be faster than the hydrogenation with both rates tending to be closer at high temperature, in perfect quantitative agreement with the observations reported by Kellner and Bell (11), Mori *et al.* (12), and van Nisselrooij *et al.* (13).

*CO Adsorption/Desorption at 25°C after Reduction, Reaction, and Regeneration*

Figure 2 shows the infrared spectra obtained by subtracting the spectrum recorded at room temperature under helium to the spectra recorded under 1 kPa of CO: (i) before reaction, (ii) after 4 h of reaction, and (iii) after regeneration by TPH (curves a, b, and c, respectively). Two CO bands were found at 2080 (shoulder) and 2050 $cm^{-1}$ in the 2100–2000 $cm^{-1}$ range corresponding to linear species and a broad band at around 1900 $cm^{-1}$ with a poorly defined shoulder at around 1820 $cm^{-1}$ in the 2000–1700 $cm^{-1}$ range, corresponding to bridged carbonyl species. A precise assignment is proposed in the discussion section (Table 4). As shown in Fig. 2, a general and strong decrease in the intensity of all the bands was observed after reaction (spectrum b). After TPH treatment (spectrum c), the bands were partly restored, except the high frequency ones at ca 2080 and 2050 $cm^{-1}$.

The dynamics of CO adsorption and desorption at room temperature was followed by recording continuously the spectra as a function of time. Figure 3 reports selected spectra corresponding to different times of CO adsorption (a)–(g) and desorption (h). At short contact time under CO/He atmosphere (a)–(e), the low frequency bands developed first and remained larger than the high frequency ones. For the latter, it can be noted that the band at 2075 $cm^{-1}$ developed before the 2047 $cm^{-1}$ one (e)–(f). After around 1 h on CO/He stream, the high frequency bands (mostly the 2047 $cm^{-1}$ one) became prominent (g). No significant shift in frequency was observed for these bands. After replacing CO/He by pure He (h), the high frequency bands strongly decreased (mostly the 2047 $cm^{-1}$ one) and a band at 2012 $cm^{-1}$ was observed. In contrast, the low frequency band only slightly decreased with a shift of around 15 $cm^{-1}$ to lower frequency.

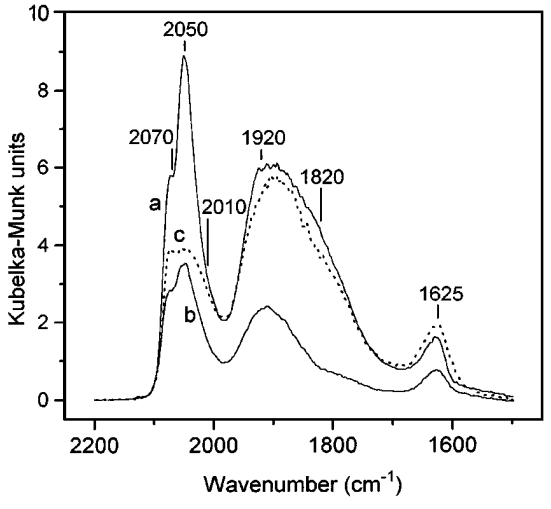


**FIG. 2.** Infrared spectra of irreversibly adsorbed CO at room temperature over $Ni/SiO_2$ (a) before reaction, (b) after 4 h of reaction, and (c) after regeneration with hydrogen.

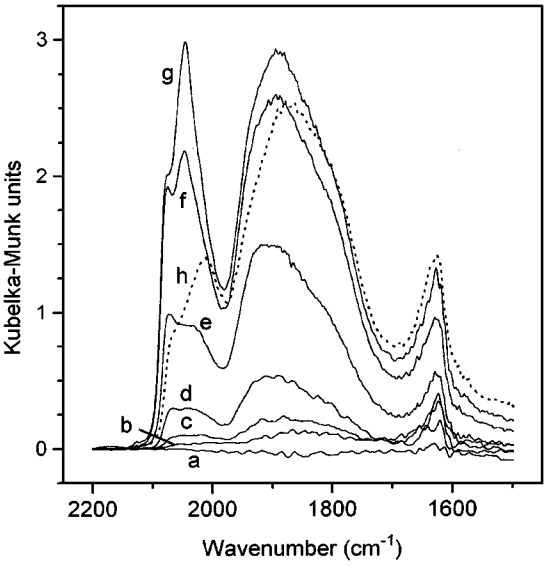


**FIG. 3.** Infrared spectra of CO chemisorbed over $Ni/SiO_2$ under 1 kPa of CO at room temperature (a) before adsorption (b) after 4.1 min adsorption, (c) 7.2 min, (d) 9.9 min, (e) 17.0 min, (f) 36.0 min, (g) 54.5 min, (h) after He flush for 5 min.

*In situ DRIFT Spectroscopy under Reaction Conditions*

After loading the DRIFT cell with a fresh catalyst and reducing it *in situ*, the temperature was fixed at 230°C and the pure He flow was switched to the reacting mixture $CO/2H_2$ at a flow rate of 3.6 liters $h^{-1}$. It was checked that the initial activity and the ageing process with time on-stream was similar to what was observed in the tubular micro-reactor as reported in Fig. 1. The spectra were recorded continuously and corrected for the spectrum recorded under pure helium stream. Figure 4 reports some of these subtracted spectra as a function of time on-stream.

In the range of hydroxyl groups (not reported in Fig. 4), a band at 3745 $cm^{-1}$ was observed on the reduced sample before reaction, which could be assigned to the free silanol groups of the silica (after checking the DRIFT spectra of the silica). After admitting the reacting mixture, this band decreased, resulting in a negative peak on the subtracted spectra. A weak but large band around 3400 $cm^{-1}$ developed in the mean time, together with a band at ca 1620 $cm^{-1}$, as expected from the water formation arising from the methanation reaction (Fig. 4). In this respect the decrease of the isolated silanol groups could be explained by the hydrogen bonding due to the silica hydration. A narrow band was also observed at 3020 $cm^{-1}$, which could be assigned to the produced gaseous methane. No other C–H bands over the range 2720–3120 $cm^{-1}$, revealing the presence of stable adsorbed hydrocarbons were detected.

Beside these bands, the introduction of the reacting mixture mostly resulted in the appearance of bands in the carbonyl range as can be seen in Fig. 4. They were decomposed to several peaks at ca 2180, 2110, 2070, 2010, 1920, and 1820 $cm^{-1}$. Note that these frequencies may vary within a range of around $\pm 5 cm^{-1}$, depending on the time on-stream and the chosen deconvolution parameters. The surface area of these bands is reported as a function of time on-stream in Fig. 5 (the separation of peaks at 2060 and 2010 $cm^{-1}$, on the one hand, and at 1917 and 1810 $cm^{-1}$, on the other hand, being not fully unambiguous, the areas of these two series were lumped together in this figure). As a general trend, all the bands increased rapidly within the very first minutes after admitting the reacting mixture, then decreased regularly with time on-stream, except for the highest frequency doublet (2180 and 2110 $cm^{-1}$), ascribed to the gaseous CO. Within the reasonable assumption of similar extinction coefficients for all the carbonyl bands, the decrease of the concentration of carbonyl adspecies with time on-stream can be evaluated to a factor of 6–7.

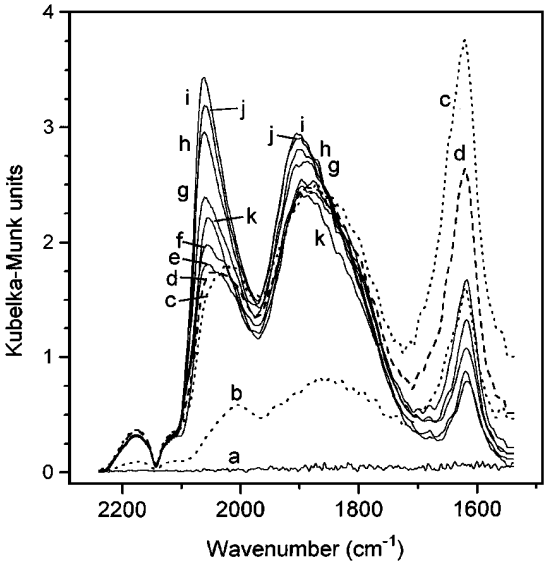


**FIG. 4.** DRIFT *in situ* spectra as a function of reaction time (in min) obtained during the CO hydrogenation over $Ni/SiO_2$ at 230°C after (a) 0 min, (b) 0.13, (c) 0.20, (d) 0.27, (e) 0.40, (f) 0.53, (g) 0.94, (h) 2.57, (i) 9.80, (j) 45.00, (k) 240.00.

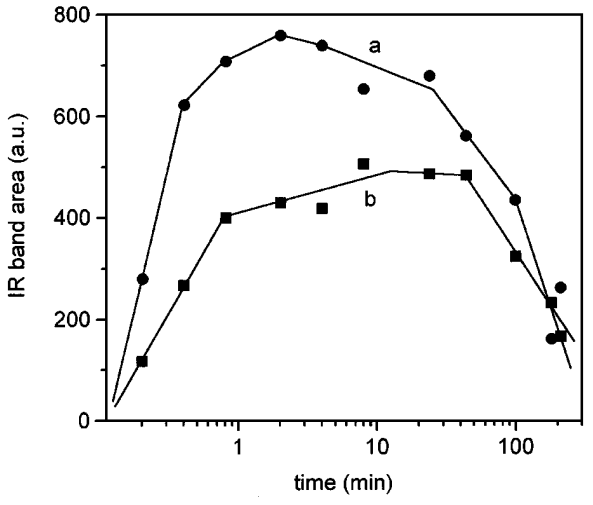


**FIG. 5.** Areas of the infrared CO bands as a function of reaction time: (a) bands at 1950 and 1810 $cm^{-1}$ (bridged + multibonded), (b) bands at 2060 and 2010 $cm^{-1}$ (linear + subcarbonyl).

*SSITK Experiments*

Figure 6 reports the normalized transient curves obtained during the SSITK experiments (switch from $^{12}CO/2H_2$ to $^{13}CO/2H_2$) after 5 min and 4 h on-stream and after regeneration with hydrogen treatment. In each case, a delay was observed between the responses of the He inert tracer and of CO, as generally observed for similar experiments carried out for CO hydrogenation (7, 14–17). This is indicative of the presence of a reservoir of adsorbed CO in equilibrium with CO in the gas phase during the reaction course. As can be seen, the delay was large on the fresh catalyst but markedly decreased after 4 h on-stream or after regeneration (TPH), in agreement with the changes observed above on carbonyl IR band intensity. The concentration of

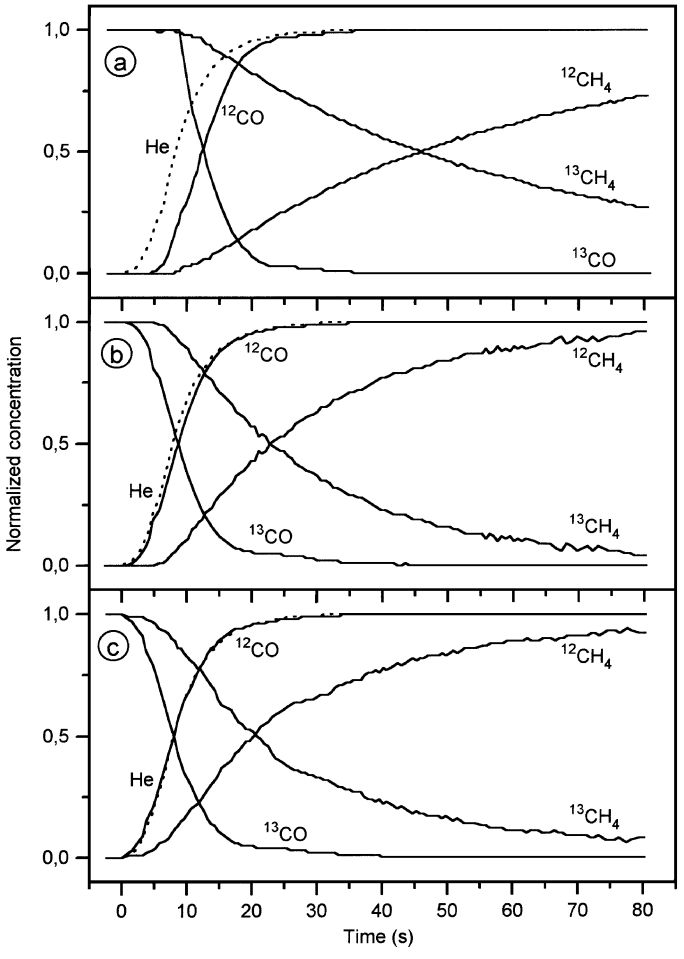


**FIG. 6.** Normalized concentration of He, $^{12}CO$, $^{13}CO$, $^{12}CH_4$, $^{13}CH_4$ as a function of time obtained during SSITK experiments at 230°C involving the switch $^{13}CO + H_2 \rightarrow {}^{12}CO + H_2$: after (a) 5 min, (b) 4 h of reaction, and (c) after regeneration.

reversibly adsorbed CO, $N_{CO_{ads}}$, was directly obtained from the product of the flow rate of CO at the reactor exit by the above delay, $\tau_{CO}$, which represents the average residence time of CO on the surface (3, 10).

Major changes with time on-stream were also observed for the delays between the methane and the inert tracer responses. They represent the mean lifetime $\tau_{CH_x}$ of the active intermediates giving $CH_4$ (referred to as $CH_x$) accumulated on the surface under steady-state conditions (3, 7, 10). Assuming that the methanation reaction is pseudo-first-order and minimizing the time effect due to the reversible adsorption of CO (by measuring $\tau_{CH_x}$ between the CO, instead of the inert tracer, and the methane responses) the rate of methane production, $r_{CH_4}$, the concentration of the methane precursors, $N_{CH_x}$, and the mean lifetime $\tau_{CH_x}$ are related by the relationship: $r_{CH_4} = N_{CH_x}/\tau_{CH_x}$ (3, 7, 10). The respective data are reported in Table 3.

Thus, at 230°C, the concentration of adsorbed CO, $N_{CO_{ads}}$, decrease by a factor of 9–10 after 4 h on-stream. This factor is in remarkable agreement with the one deduced from the decreased in CO IR band intensity (around 6–7) observed in Fig. 5, within the uncertainty of the two different methods. The concentration of methane precursors, $N_{CH_x}$, was also found to decrease markedly during this startup period (Table 3).

The sensitivity of the transient responses to the temperature was investigated by varying the temperature of reaction in the range 230–350°C after reaching a pseudo-stabilized state after 4 h on stream and by decreasing the contact time at high temperature to stay within the nondiffusional range (lower catalyst loading). It was checked that the changes in activity during the time necessary for the transient experiments was negligible. The transient curves clearly showed that the delay between carbon monoxide and methane ($\tau_{CH_x}$) strongly decreased with the temperature, while the delay between the inert tracer and the CO responses ($\tau_{CO}$) stayed rather stable, as shown in Table 3. Consequently, the surface concentration of adsorbed CO, $N_{CO_{ads}}$, was found to slightly decrease with temperature, while the concentration of methane precursors, $N_{CH_x}$, increased regularly (Table 3). It was checked that the specific rate and surface concentrations did not vary as a function of contact time. The apparent activation energies corresponding to the rate of methane production and to the changes in surface concentration for these adspecies are reported in Table 3.

In order to find out if a relationship existed between the reservoir of surface (or subsurface) stable carbon which formed the carbide-like monolayer (Fig. 1) and the active intermediates leading to methane formation under steady-state conditions, the following experiment was performed, as depicted in Fig. 7. The catalyst was flushed with helium for 1 h before the isotopic switch, according to the sequence $^{12}CO/2H_2 \rightarrow He \rightarrow {}^{13}CO/2H_2$. During the switch $He \rightarrow {}^{13}CO/2H_2$, a transient formation of $^{12}CH_4$ was observed, which corresponded to a large part of the amount of $CH_x$ determined by the previous SSITK experiments (23 vs 38 $\mu$mol/$g_{cat}$, Table 3), while no delay was observed between the transient curves of labelled CO and methane. This experiment demonstrated that the carbide-like monolayer (formed of $^{12}C$ in the present experiment) constituted a reservoir for the reacting intermediates, which tends to rule out any scheme assuming the direct hydrogenation of CO adspecies into methane.

SSITK experiments were also carried out by switching from $H_2$ to $D_2$ at the reactor inlet under methanation conditions. Due to the complex superposition of masses (the series of $CH_xD_{4-x}$ methane molecules corresponds to the series of $H_yD_{2-y}O$ water molecules), no precise information about the accumulation of partially hydrogenated adspecies was available. However, it was clearly revealed by observing the transient formation of HD during the switch (Fig. 8) that a fast dissociative adsorption/desorption

**TABLE 3**

**Rate of Methane Production and Amounts of Reversibly Adsorbed CO and of Reacting Intermediates $CH_x$ Determined from SSITK Experiments at Various Times On-Stream and Reaction Temperature**

| Time on-stream (min) | T (°C) | Rate of $CH_4$ production ($\mu$mol/s $g_{cat}$) | SSITK delays[a] (s) | | Surface species concentration ($\mu$mol/$g_{cat}$) | | Surface coverage | |
|---|---|---|---|---|---|---|---|---|
| | | | $\tau_{CO}$ | $\tau_{CH_x}$ | $N_{CO_{ads}}$ | $N_{CH_x}$ | $\theta_{CO}$ | $\theta_{CH_x}$ |
| 5 | 230 | 2.78 | 13.6 | 133.5 | 2480 | 371.0 | | |
| 240 | 230 | 1.25 | 1.4 | 31.0 | 255 | 37.7 | 0.88 | 0.08 |
| 240 | 250 | 2.78 | 1.4 | 17.5/19.2 | 249 | 48.9 | 0.85 | 0.09 |
| 240 | 270 | 6.21 | 1.3 | 13.2/13.2 | 220 | 81.9 | 0.76 | 0.18 |
| 240 | 290 | 13.87 | 1.3 | 6.9 | 200 | 108.5 | 0.74 | 0.19 |
| 240 | 300 | 19.55 | 1.4 | 5.6 | 216 | 129.9 | 0.69 | 0.24 |
| 240 | 350 | 85.16 | 1.2 | 1.6 | | 151.7 | 0.63 | 0.30 |
| $E_a$ (kcal/mol) | | 22.1 | | | −1.5 | 6.7[b] | | |

[a] After correction from the noncatalytic delay due to the chromatographic effect along the setup lines.
[b] Average value over the 230–350°C range, since this energy tends to decrease with temperature.

equilibrium established between the gaseous hydrogen and the metallic surface (it was checked that no similar transient was observed over pure silica).

## DISCUSSION

The experimental data are discussed by considering separately (i) the changes in surface properties observed during the first hours on CO hydrogenation stream, before reaching a pseudo-steady-state catalytic regime and (ii) the kinetic and mechanistic information obtained on aged catalysts, i.e., under quasi-steady-state conditions.

### *Changes in Surface Properties with Time On-Stream and after Regeneration*

*Characterization by CO adsorption at room temperature.* By referring to the abundant literature about carbonyl vibrations, the DRIFT observations upon CO adsorption at room temperature lead to the following assignments, as summarised in Table 4.

After adsorption of CO at room temperature, two main bands at ca 2070 and 2045 $cm^{-1}$ were observed within the range of high frequency linear carbonyl species (2080–2040 $cm^{-1}$) which presented frequencies little dependent either on the state of the catalyst (fresh, aged, or regenerated), or on the surface concentration (under CO adsorption, or after He flush). They are characteristic of polycarbonyl species (18–22):

(i) The band at ca 2070 $cm^{-1}$ which was observed under CO pressure mainly on the fresh sample, but also after ageing and regeneration (Figs. 2a, b, c) can be assigned to subcarbonyl nickel species $Ni(CO)_n$ ($n = 2, 3$) preferentially formed on low co-ordinated Ni atoms (corner, step, or kink positions). In this respect, the decrease of this band after CO hydrogenation (spectra b and c) correspond logically to the smoothing effect of the nickel particles with the preferential development of ⟨111⟩ planes during the sintering process which occurred under reaction conditions (5, 22).

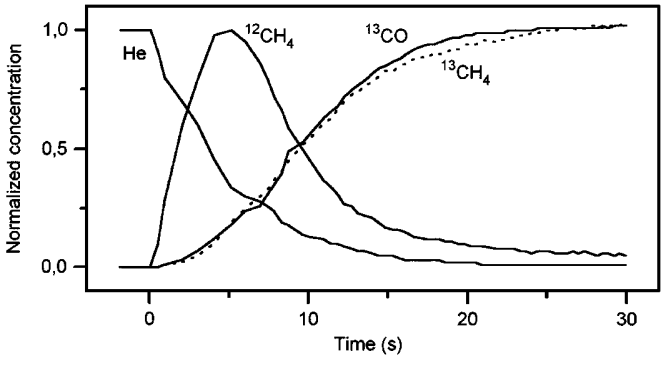


**FIG. 7.** Normalized concentration of He, $^{12}CO$, $^{13}CO$, $^{12}CH_4$, $^{13}CH_4$ as a function of time obtained during NSSTK experiments at 230°C involving the switches $^{12}CO + H_2 \rightarrow$ He (10 min) $\rightarrow {}^{13}CO + H_2$.

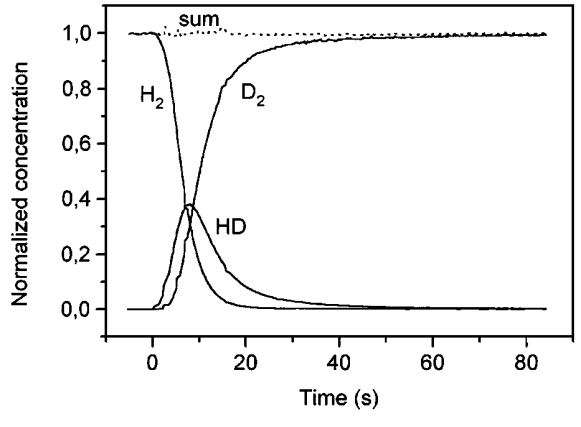


**FIG. 8.** Normalized concentration of $H_2$, $D_2$, and HD as a function of time obtained during SSITK experiments at 230°C involving the switch $^{12}CO + H_2 \rightarrow {}^{12}CO + D_2$.

**TABLE 4**

**Assignment of the CO Bands Observed by DRIFT Spectroscopy**

| Species | | Wavenumber range ($cm^{-1}$) | References | *In situ* observed wavenumber ($cm^{-1}$) |
|---|---|---|---|---|
| Sub (di- or tri-) carbonyl | $Ni(CO)_{2-3}$ | 2080–2050 | 18, 19 | 2080–2075 |
| Silica supported tetra-carbonyl | $Ni(CO)_4$ | 2045 | 20 | 2045 |
| Linear mono-carbonyl | Ni–CO | 2010–2000 | 18–21 | 2010 |
| Bridged mono-carbonyl | $Ni_2$–CO | 1950–1880 | 18–21 | 1910–1880 |
| Multibonded | $Ni_4$–CO | 1875–1800 | 18–21 | 1820 |

(ii) The band at 2045 $cm^{-1}$ was mainly observed on the fresh catalyst and under CO pressure (spectrum a in Figs. 2 or f and g in Fig. 3), but disappeared upon He flush (spectrum h in Fig. 3). Moreover, it appeared under CO pressure after the formation of the subcarbonyl species (Fig. 3). From this behavior, it can be assigned to $Ni(CO)_4$ species physically adsorbed on the catalyst surface (nickel and/or silica) (22). Thus, these species, highly unstable since they are essentially observed at room temperature, are considered as responsible for the nickel transfer from particle to particle, forming the atomically dispersed phase involved in the Ostwald ripening process modelled in (5). As for the previous subcarbonyl band, the decrease of the tetracarbonyl band intensity on an aged catalyst corresponds to the slowdown of the sintering process with time on-stream (5).

After desorption of the previous tetracarbonyl species at room temperature (spectrum h in Fig. 3), a band was revealed at ca 2012 $cm^{-1}$. In contrast to the previous polycarbonyl bands its frequency regularly decreased with the CO coverage (from 2012 to ca 2000 $cm^{-1}$ with time under He flush and thereafter during desorption at increasing temperature). This is characteristic of linear monocarbonyl species adsorbed on the Ni particles (Table 4).

Within the range of lower frequency (1980–1700 $cm^{-1}$) the poorly defined broad band could be decomposed into two distinct vibrations: one at ca 1900 $cm^{-1}$ and a shoulder at ca 1820 $cm^{-1}$. Upon CO adsorption, the latter tended to form first (Figs. 3b, c) and upon CO desorption it was found more stable than the former (Fig. 3 h). From these observations and in accordance with literature assignments on Ni single crystals (23–25), the band at ca 1900 $cm^{-1}$ can be attributed to $Ni_2CO$ bridged species and the shoulder at 1820 $cm^{-1}$ to multibonded $Ni_4CO$ species which would be preferentially formed on a bare surface (21).

Within the frame of the previous assignments, the major decrease of the CO adsorption on the aged sample (more specifically affecting the multibonded species by comparison with the polycarbonyl species (Fig. 2b)) cannot be ascribed to the loss of surface area arising from particle sintering since these bands were restored after $H_2$ regeneration treatment (Fig. 2c). Moreover, by extrapolating to zero coverage the shift in frequency of the bridged species (by following the spectrum changes at increasing desorption temperature), the following values were obtained: 1995, 2004, and 1994 $cm^{-1}$ for samples before reaction, after reaction, and after carbon removal, respectively. This confirmed that a major change in adsorption properties occurred when the initially metallic surface was carbided, this change being reversible after carbon removal in the regeneration step.

Thorough investigations have been reported on the adsorption properties of carbided single crystals. The CO adsorption was found to strongly decrease on ⟨111⟩ and ⟨110⟩ carbided nickel surfaces (26, 27) and even be suppressed on the ⟨100⟩ surface, revealing a marked weakening of the metal–CO bond in the presence of surface carbon. Moreover, only linear CO was observed on a carbided Ni(110) surface (27). In this respect, the preferential decrease of the multibonding adsorption for the present $Ni/SiO_2$ catalyst would mean that the flat surfaces which develop with time on-stream are homogeneously carbided while the low co-ordinated Ni atoms, where the linear adsorption is favoured would be less electronically modified by the carbon deposits.

*Characterization by $H_2/D_2$ exchange.* The above changes in surface properties after carbon deposition were also directly revealed by the large decrease in the rate of $H_2/D_2$ equilibration and the increase of activation energy, these values being restored to their initial level after carbon removal by $H_2$ regeneration (Table 1). Again these results are in accordance with results obtained on single crystals showing a marked decrease of the hydrogen adsorption on a precarbided surface. Thus, a decrease of two orders of magnitude was observed on a ⟨110⟩ carbided Ni surface and the weakening of the Ni–H bonding was attributed to the displacement of valency electrons of nickel to the strong Ni–C bonds of the carbide (26).

*Characterization under reaction conditions.* From the deconvolution of the IR spectra and after a statistical analysis of the changes with time of stream, the following CO bands were observed under reaction conditions: 2180, 2110, 2070, 2010, 1920, and 1820 $cm^{-1}$. The two former bands, stable with time on-stream, are due to gaseous CO and will not be considered further. From Table 4, the four remaining bands were attributed to subcarbonyl, linear, bridged, and

multibonded species, respectively. As shown in Fig. 5 reporting the evolution of peak surface areas as a function of reaction time, the intensity of both high and low frequency groups increased rapidly in the very first minutes, which corresponded to the expected completion of the surface coverage by CO adspecies, then decreased progressively to stabilize after some hours on-stream. This decrease and further stabilisation in CO coverage can be directly related to the formation of the carbided layer, which builds up in the same time interval (Fig. 1). These changes in IR spectra have also to be related to the progressive sintering process which will regularly decrease the adsorbed CO signal. It can be noted more precisely on Fig. 5 that the multibonding adsorption forms (low frequencies) are more affected by the carbide surface buildup than the single bonding species (essentially polycarbonyl and linear at high frequency) in accordance with the statements deduced from CO adsorption at room temperature.

*Surface Properties under (Pseudo) Steady-State Conditions*

After having reached a pseudo-steady-state regime within 3–4 h on stream, which corresponded to the completion of the carbidic layer and the initial sintering process, the working surface appeared to be covered by a mixture of subcarbonyl, linear, bridged, and multi-bonded CO species. A precise Ni/CO stoichiometry can hardly be derived from this statement; however, by assuming the same extinction coefficient for all the adspecies, an evaluation of the distribution of all these adspecies can be attempted on the basis of the spectra deconvolution (Table 5).

From the value of $Ni_s$/CO stoichiometry assumed for each carbonyl adspecies (Table 5), a mean stoichiometry of 1.7 $Ni_s$/CO can be deduced from the evaluated distribution of CO adspecies for the aged catalyst.

Let us focus now on the specific surface concentration of adsorbed CO, $N_{CO_{ads}}$, and of reacting intermediates, $N_{CH_x}$, evaluated from SSITK analysis. Table 3 clearly shows that $N_{CH_x}$ increased significantly with temperature, while $N_{CO_{ads}}$ slightly decreased. The question arises now about the average value of the CO bonding (i.e., the mean $Ni_s$/CO stoichiometry) and about the possible molecular structure of the reacting intermediate $CH_x$ (i.e. the $Ni_s/CH_x$ stoichiometry), both informations being necessary to calculate the surface coverages $\theta_{CO}$ and $\theta_{CH_x}$, defined as the fraction of Ni surface bonded to adsorbed CO and reaction intermediate $CH_x$, respectively.

**TABLE 5**

**Distribution of Adsorbed CO Species after 4 h On-Stream at 230°C, Evaluated from DRIFT Spectra Decomposition**

| Adspecies | $Ni(CO)_{2-3}$ | Ni(CO) | $Ni_2CO$ | $Ni_4(CO)$ |
|---|---|---|---|---|
| Distribution (%) | 27 | 16 | 40 | 17 |
| $Ni_s$/CO | 0.4[a] | 1 | 2 | 4 |

[a] An average number of 2.5 CO per surface atom of nickel is assumed for the subcarbonyl species.

*Nature of the Active Sites and Mechanism*

Due to (i) the nickel particles smoothing (with the preferential development of ⟨111⟩ planes by sintering) and (ii) the buildup of a nickel carbide monolayer during the first hours on-stream, it is assumed that the working surface of an aged catalyst presents a rather uniform reactivity, little dependent on plane orientation and/or of specific atoms in odd crystallographic position (low coordination atoms, mostly occupied by polycarbonyl adspecies, therefore unfavored for C–O activation). This statement is supported by a mathematical analysis of the SSITK curves of the methane responses (Figs. 7 and 8) which appeared to be essentially exponential, i.e. to reflect a homogeneous pool of intermediates with a single reactivity (3, 7, 14, 15). Inferentially, a statistical model like the one proposed by Martin and Dalmon (9) which considers that the reacting surface is homogeneous towards the CO hydrogenation reaction can be considered to analyse the present kinetic data.

As mentioned in the Introduction, the reaction rate in this model is directly related to the probability of collision between two species: (i) molecular hydrogen and (ii) a surface compound formed by an active surface carbon bound to an ensemble composed of W adjacent nickel atoms free from inactive molecular adsorbed CO. The rate equation can be written as

$$r = K_o \exp(-E_o/RT) P_{H_2} (1 - \theta_{CO})^W. \quad [3]$$

The term $P_{H_2}$ reflects the order one with respect to $H_2$ pressure, determined experimentally (9). The term $(1-\theta_{CO})^W$ reflects the negative orders with respect to CO pressure and represents the concentration of active sites, i.e., the fraction of Ni surface occupied by reacting intermediates, $\theta_{CH_x}$, determined from the present SSITK analysis:

$$(1 - \theta_{CO})^W = \theta_{CH_x}. \quad [4]$$

Indeed such a formalism implicitly assumes that the H coverage does not interfere with the CO coverage for determining the active site concentration. Let us discuss this point.

The buildup of a carbide layer was shown to strongly decrease the Ni–H bond energy, as clearly shown by a decrease by two orders of magnitude of the rate of $H_2/D_2$ exchange (Table 1). Moreover, from classical volumetric experiments, the hydrogen coverage of a freshly reduced $Ni/SiO_2$ (in the absence of CO) was found to lie between 0.3 and 0.4 between 200 and 300°C (25). It can therefore be deduced from the above observations that under reaction conditions

(adsorption in competition with CO on a carbided surface) the actual hydrogen coverage (not measurable directly by H tracing experiments due to the superimposed signal of OH groups) should not affect the surface coverage by CO and reacting intermediate adspecies. Adsorbed atomic species of hydrogen exist, however, under these conditions to account for the fast hydrogen adsorption/desorption equilibrium revealed by the SSITK experiment in Fig. 8.

The measured surface concentrations of CO and $CH_x$ adspecies reported in Table 3 ([CO] and [$CH_x$], respectively, expressed in $\mu$mol/$g_{cat}$) can be converted into surface coverages ($\theta_{CO}$ and $\theta_{CH_x}$, respectively) through the actual stoichiometries $Ni_s/CO = A$ and $Ni_s/CH_x = W$ and the concentration of surface nickel atoms, [$Ni_s$], as follows:

$$\theta_{CO} = A[CO]/[Ni_s], \quad \theta_{CH_x} = W[CH_x]/[Ni_s]. \qquad [5]$$

By combining Eqs. [4] and [5], Eq. [6] can be derived:

$$[CH_x] = ([Ni_s]/W)(1 - A[CO]/[Ni_s])^W. \qquad [6]$$

The concentration of surface nickel atoms, [$Ni_s$], was measured on the similarly aged catalyst by $H_2$ volumetry, magnetic measurements, and TEM as reported in part 1 of this work (5) and was found to be around 600 $\mu$mol $Ni_s/g_{cat}$. The stoichiometric coefficients A and W being directly related to the rate-determining step of the methanation were assumed not to vary significantly over the studied temperature range.

On the above basis, the stoichiometric coefficients A and W were calculated by applying a nonlinear regression procedure from the experimental values of [$CH_x$] and [CO] in Table 3. An excellent fit (correlation coefficient = 0.99) was obtained over the whole temperature range, giving the values:

$$A = Ni_s/CO = 2.1, \quad W = Ni_s/CH_x = 1.2.$$

It can be stressed that the bonding coefficient $A = Ni_s/CO$ thus determined from SSITK experiments compares quite well with the value determined independently from *in situ* IR spectroscopy (1.7).

From the A and W values, the coverages $\theta_{CO}$ and $\theta_{CH_x}$ were calculated by means of Eq. [5] and their values are reported in Table 3 and plotted versus the reciprocal temperature in Fig. 9.

A precise description of the working nickel surface can be derived from these data:

—at low temperature, the surface is predominantly covered with CO ($\theta_{CO} = 0.88$ ML) while only a small fraction of the surface is occupied by reacting intermediates ($\theta_{CH_x} = 0.08$ ML).

—at increasing temperature, $\theta_{CO}$ slowly decreases down to 0.6 ML at 350°C while $\theta_{CH_x}$ tends to get closer to the carbide-like monolayer ($\theta_C = 0.4$) shown to be stable under the investigated reaction conditions.

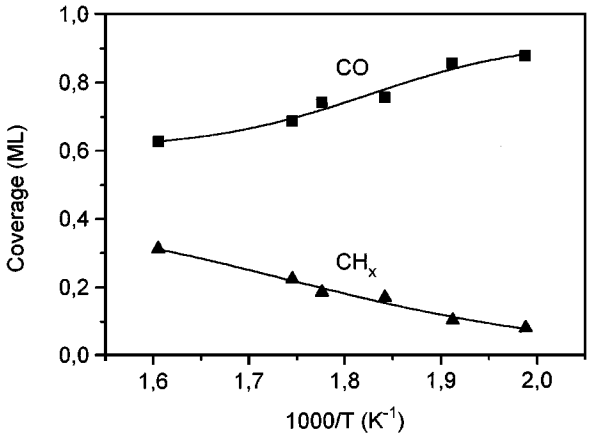


**FIG. 9.** Changes in the CO and $CH_x$ (reacting intermediates leading to methane) coverages (monolayer) as a function of the reciprocal temperature.

From these results, the following scheme can be proposed for the CO hydrogenation over the $Ni/SiO_2$ catalyst:

After an initial period of carbon deposition, fast particle sintering, and smoothing, the reacting surface can be described as a monolayer of nickel carbide, mainly covered by CO adspecies which present an average bonding stoichiometry of 2 $Ni_s$/CO. The rate of hydrogenation is controlled by the probability for a hydrogen molecule to collide with an ensemble of one to two Ni atoms free from adsorbed CO. This active site, statistically determined by the CO coverage, allows a carbon atom belonging to the carbidic layer (thus probably underneath the Ni surface as proposed for single crystal studies (26, 27)) to be hydrogenated by the dissociated hydrogen on the free Ni atoms. As soon as a carbon atom is extracted from the carbidic overlayer and hydrogenated, a CO adspecies dissociates (most probably the $Ni_4CO$ multibonded form with a weakened C–O bond vibrating at 1820 $cm^{-1}$) and regenerates the carbidic layer. In the mean time, the O atom arising from the CO dissociation is rapidly hydrogenated into OH and further on it is dehydroxylated as $H_2O$, as observed by DRIFT.

In this respect, let us comment on the KIE, which has been confirmed experimentally in the present study. First, it rules out any RDS restricted to the single CO bond activation, which confirms that the slow steps are dealing with the carbonaceous adspecies hydrogenation. However, the C–H bond activation is indeed expected to be easier than the C–D bond activation. Therefore this inverse KIE suggests a complex combination of kinetic and equilibrium isotopic effects which compensate for the time, as proposed by Kellner and Bell (11) and by van Nisselrooij *et al.* (13). From statistical thermodynamics the surface coverage by deuterated CD species was found higher than the one by CH species, thus overcompensating for the normal KIE occurring during the further hydrogenation into carbene species (13). Such a suggestion applies well to our mechanism

since the overall RDS step we propose assumes elementary presteps such as the fast adsorption/desorption equilibrium of hydrogen (experimentally confirmed by the rapid $H_2/D_2$ isotopic exchange under methanation conditions). A fast and reversible step dealing with the initial hydrogenation of carbidic species to CH species, later slowly hydrogenated into $CH_2$ carbene, as often proposed in the literature (4, 11, 13), remains quite compatible with the present mechanistic scheme. This leads us to define the intermediate active species as $CH_x$.

As originally pointed out by Temkin (29), the apparent activation energy $E_a$ has to be corrected from the energy related to the reacting adspecies (Table 3). If one neglects the adsorbed hydrogen species which should not play any significant kinetic role, as discussed above, this leads to the true activation energy $E_o$ in Eq. (3):

$$E_o = E_a - E_{adspecies} = 22.1 - 6.7 = 15.4 \text{ kcal}. \quad [6]$$

This value of the true activation energy is close to the value of 17 kcal/mol derived from the kinetic analysis reported by Martin and Dalmon (9).

On the basis of Eq. [3], it was also possible to evaluate the frequency factor $k_o$,

$$k_o = 4.4 \times 10^{18} \text{ molecules/s cm}^2_{Ni} \text{ Torr}.$$

It may be of interest to compare this frequency factor with the number of hydrogen molecules colliding with the nickel surface calculated from the kinetic theory of gases,

$$v = 1.1 \times 10^{21} \text{ collisions/s cm}^2_{Ni} \text{ Torr}.$$

The latter is larger than the former by a factor 250, suggesting that the efficiency coefficient of the CO hydrogenation reaction is 1/250, a ratio quite plausible for a gas–solid reaction involving several complex elementary steps.

Finally, the kinetic trends determined above can be compared to the ones proposed by Alstrup (4) from his microkinetic approach. Quite good agreement is achieved if one considers the CO coverage at low temperatures (0.90 in (4), compared to 0.88 in the present study) and the active carbon coverage (assumed to be 0.05 in (4), compared to 0.08 in the present study). However, a major discrepancy between the two models lies in the fact that the active carbon coverage is assumed to be constant over a large range of temperatures in (4), while it was demonstrated in the present study that this coverage actually increased with the reaction temperature, up to a level where the entire carbidic overlayer tends to participate directly to the hydrogenation process, due to the decrease in the inhibiting role of the CO coverage. Furthermore, the model from Alstrup is based on a simplified concept of active sites (one surface atom per adsorbed species, whatever be its nature). However, it clearly appears from this study that the sites stoichiometry are rather different, either for the CO adspecies (a large range of bonding stoichiometries with an average value around 2 $Ni_s$/CO) or for the reacting intermediates which require 1 or 2 $Ni_s$ adjacent free from CO for the hydrogenation of a carbidic and/or a CH species. In addition, the microkinetic model developed in (4) is unable to predict orders with respect to CO pressure smaller than $-1$ which are indeed observed at low reaction temperatures. Highly negative orders are brought about by the present ensemble model (9) which, from this viewpoint, appears as a plausible alternative.

## CONCLUSION

This study has confirmed the major interest of applying *in situ* transient techniques for understanding the reaction mechanism of the CO hydrogenation over a $Ni/SiO_2$ catalyst, combined with the ageing process.

It was first confirmed that the CO hydrogenation induces a deep restructuring of the nickel phase with a selective development of dense planes. During the startup period the CO coverage increases rapidly, goes through a maximum, then decreases to a steady-state value around 0.8 ML after some hours of reaction at 230°C. The formation of subcarbonyl species $Ni(CO)_x$ with $x = 2$ or 3 plays a crucial role in the sintering and smoothening of the nickel particles. A second key phenomenon occurs simultaneously which corresponds to the progressive buildup of a carbide-like monolayer up to an equilibrium stoichiometry $C/Ni_s = 0.40$. This leads to a weakening of the Ni–CO and Ni–H bond strengths. This form of carbon has to be distinguished from the reacting intermediates $CH_x$ leading to methane formation. Thus, the surface coverage with the latter, $\theta_{CH_x}$, is found to be low at 230°C (0.08 ML), but increases significantly with the temperature up to values closer to the concentration of surface carbide ($\theta_C = 0.40$ ML).

These experimentally measured surface coverages and their changes with temperature were rationalized within the framework of a model assuming that the reacting site is composed of one to two nickel atoms free from adsorbed CO which allow the hydrogenation of a carbon atom belonging to the carbidic reservoir to proceed. The methanation rate is thus determined by the probability of the collision of a gas phase hydrogen molecule with such an active site, the concentration of which depends on the CO coverage. This scheme does not preclude elementary steps of hydrogen dissociation for hydrogenating surface carbon. Such a "statistical" kinetic control tends to rule out any structure sensitivity effect, at least for the studied range of nickel dispersion.

## ACKNOWLEDGMENT

CMA gratefully acknowledges a postdoctoral fellowship granted by the Spanish Ministerio de Educación y Cultura.

## REFERENCES

1. *In situ* methods in catalysis, *Catal. Today* **9**, 2 (1995).
2. Happel, J., "Isotopic Assessment of Heterogeneous Catalysis," Academic Press, Orlando, FL, 1986.
3. Shannon, S. L., and Goodwin, J. G., Jr., *Chem. Rev.* **95**, 677 (1995).
4. Alstrup, I., *J. Catal.* **151**, 216 (1995).
5. Agnelli, M., Kolb, M., and Mirodatos, C., *J. Catal.* **148**, 9 (1994).
6. Goodman, D. W., Kelley, R. D., Madey, T. E., and White, J. M., *J. Catal.* **64**, 479 (1980).
7. Biloen, P., *J. Mol. Catal.* **21**, 17 (1983); Biloen, P., Helle, J. N., Van den Berg, F. G. A., and Sachtler, W. H. M., *J. Catal.* **81**, 450 (1983).
8. Mirodatos, C., Praliaud, H., and Primet, M., *J. Catal.* **107**, 275 (1987).
9. Dalmon, J. A., and Martin, G. A., *J. Catal.* **84**, 45 (1983).
10. Mirodatos, C., *J. Phys. Chem.* **90**, 481 (1986). [*Catal. Today* **9**, 83 (1991); *in* "Catalyst Characterization" (B. Imelik and J. C. Vedrine, Eds.), p. 651. Plenum, New York, 1994]
11. Kellner, C. S., and Bell, A. T., *J. Catal.* **67**, 175 (1981).
12. Mori, T., Masuda, H., Imai, H., Miyamoto, A., Baba, S., and Yurakami, Y., *J. Phys. Chem.* **86**, 2753 (1982).
13. van Nisselrooij, Luttikholt, J. A. M., van Meerten, R. Z. C., de Croon, M. H. J. M., and Coenen, J. W. E., *Appl. Catal.* **6**, 271 (1983).
14. Soong, Y., Krishma, K., and Biolen, P., *J. Catal.* **97**, 330 (1986).
15. de Pontes, G. H., Yokomizo, G. M., and Bell, A. T., *J. Catal.* **104**, 147 (1987).
16. Stockwell, D. M., Chung, J. S., and Bennet, C. O., *J. Catal.* **112**, 135 (1988).
17. Winslow, P., and Bell, A. T., *J. Catal.* **86**, 158 (1984).
18. Van Hardeveld, R., and Hartog, F., *Adv. Catal.* **75**, 1011 (1979).
19. Brum Pereira, E., and Martin, G. A., *Appl. Catal.* **103**, 291 (1993).
20. Moana Rao, K., Spoto, G., and Zecchina, A., *Langmuir* **5**, 319 (1989).
21. Martin, G. A., Primet, M., and Dalmon, J. A., *J. Catal.* **53**, 321 (1978).
22. Martra, G., Swaan, H. M., Mirodatos, C., Kermarec, M., and Louis, C., *in* "Catalyst Deactivation 1997" (C. H. Bartholomew and G. A. Fuentes, Eds.), p. 617, Elsevier, Amsterdam, 1997 [Stud. Surf. Science and Catalysis, Vol. 111]
23. Bertolini, J. C., Dalmai-Imelik, G., and Rousseau, J., *Surf. Sci.* **68**, 539 (1977).
24. Campuzano, J. C., and Greenler, R. G., *Surf. Sci.* **83**, 301 (1979).
25. Christmann, K., Shober, O., and Ertl, G. J., *J. Chem. Phys.* **60**, 4719 (1974).
26. Bertolini, J. C., and Tardy, B., *Surf. Sci.* **102**, 131 (1981).
27. McCarty, J. G., and Madix, R. J., *Surf. Sci.* **54**, 121 (1976).
28. Martin, G. A., *J. Catal.* **60**, 345 (1979).
29. Temkin, M., *Acta Physicochim. URSS* **2**, 313 (1935).